APPLIED GEOPHYSICS, Vol.12, No.4 (December 2015), P. 555-563, 13 Figures.
DOI:10.1007/s11770-015-0515-z

Using 4C OBS to reveal the distribution and velocity attributes of gas hydrates at the northern continental slope of South China Sea*

Sha Zhi-Bin[1,2], Zhang Ming[1], Zhang Guang-Xue[1], Liang Jin-Qiang♦[1,2], and Su Pi-Bo[1]

Abstract: To investigate the distribution and velocity attributes of gas hydrates in the northern continental slope of South China Sea, Guangzhou Marine Geological Survey conducted four-component (4C) ocean-bottom seismometer (OBS) surveys. A case study is presented to show the results of acquiring and processing OBS data for detecting gas hydrates. Key processing steps such as repositioning, reorientation, PZ summation, and mirror imaging are discussed. Repositioning and reorientation find the correct location and direction of nodes. PZ summation matches P- and Z-components and sums them to separate upgoing and downgoing waves. Upgoing waves are used in conventional imaging, whereas downgoing waves are used in mirror imaging. Mirror imaging uses the energy of the receiver ghost reflection to improve the illumination of shallow structures, where gas hydrates and the associated bottom-simulating reflections (BSRs) are located. We developed a new method of velocity analysis using mirror imaging. The proposed method is based on velocity scanning and iterative prestack time migration. The final imaging results are promising. When combined with the derived velocity field, we can characterize the BSR and shallow structures; hence, we conclude that using 4C OBS can reveal the distribution and velocity attributes of gas hydrates.
Keywords: gas hydrates, velocity attributes, ocean-bottom seismometer, PZ summation, mirror imaging

Introduction

Four-component (4C) ocean-bottom seismometers (OBS) have been successfully used in oil and gas exploration, gas hydrates exploration, and detecting bottom-simulating reflections (BSRs) in the continental shelf (Grion et al., 2007). Seismometers record compressional, converted, and shear waves that are used to detect gas hydrates. OBS data are used to investigate geophysical attributes for gas hydrates (Riedel et al., 2001).

Manuscript received by the Editor August 17, 2014; revised manuscript received September 12, 2015.
*This research is supported by the National Hi-tech Research and Development Program of China (863 Program) (Grant No. 2013AA092501) and the China Geological Survey Projects (Grant Nos. GZH201100303 and GZH201100305).
1. MLR Key Laboratory of Marine Mineral Resources, Guangzhou Marine Geological Survey, Guangzhou, Guangdong 510075, China.
2. Faculty of Resources, China University of Geosciences (Wuhan), Wuhan, Hubei 430074, China.
♦Corresponding Author: Liang Jin-Qiang (Email: ljinqiang@21cn.com)

Since 1999, Guangzhou Marine Geological Survey (GMGS) has been performing geological, geophysical, and geochemical investigations of gas hydrates in the northern continental slope of South China Sea (SCS). In 2007, the first gas hydrate samples were recovered, which proved the existence of gas hydrates in the northern continental slope of SCS.

To explore OBS technology for detecting gas hydrates, several 4C OBS surveys have been conducted in SCS since 2012. The survey objectives were to investigate the structure and velocity attributes of gas hydrates in the area. The most recent survey was that conducted in 2012, where 24 4C OBS stations with one hydrophone and three geophones of X, Y, and Z components were deployed and 19 stations were successfully retrieved in an area with an average water depth of 1,000 m. To overcome the large distance (over 400 m) between adjacent OBS stations, which hinders structure imaging, P- and Z-component processing is required, including station repositioning, station reorientation, noise attenuation, PZ summation, velocity model building, and mirror imaging.

Geological background

The southwestern Taiwan basin is located in northeastern South China Sea. It is characterized by geological structures that experienced two stages of significant extension at the end of Lower Cretaceous and between Oligocene and middle Miocene. During middle Miocene–Pliocene extension, subsidence was widespread, and thick marine deposits formed along the northeastern slope of South China Sea (Pang et al., 2009).

The study area is located in the central rift of the southwestern Taiwan basin (Gong et al., 2008) and is bounded by the Taiwan Canyon (Formosa Canyon) to the west and Penghu Canyon to the east. The morphology is characterized by troughs, canyons, seamounts, escarpments, slopes, scour channels, and sea knolls (Figure 1). In particular, well-developed submarine channels mostly parallel to NW-trending faults, including the classical 110-km-long Taiwan Canyon (Shi and Yan, 2011), deposit sediments from the northern slope of South China Sea to the deep sea. The central rift in the southwestern Taiwan basin is bounded by numerous secondary depressions on the north and south flanks (Yi et al., 2007). The depressions have multiple depositional centers of Lower Cretaceous, Paleogene (Paleocene, Eocene, and Oligocene), Neogene (Miocene, Pliocene), and Quaternary age (Figure 2). The corresponding source rocks contain type III kerogen at high stages of maturity. Currently, several offshore oil fields such as Niushan and Liuchongxi have been developed in the basins because of the high-quality source rocks (Li et al., 2013). The gas hydrates are predicted to exist in the Miocene–Pliocene sediments (Zhang et al., 2014a).

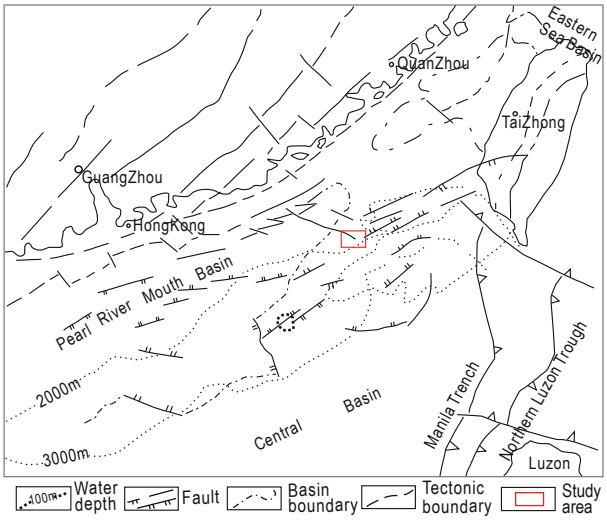

Fig.1 Geological map of northeastern South China Sea (modified after Gong et al., 2008).

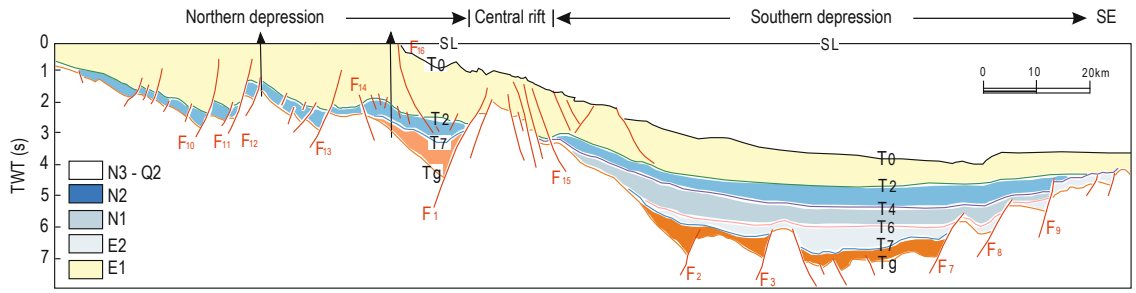

Fig.2 Cross-section of the southwestern Taiwan basin (for the section location, see Figure 1; modified after Yi, 2007).

Data acquisition

GMGS deployed "Fendou Si Hao" in July–August 2012. The sources were four GI airguns (volume 550 in3, depth 5 m, interval 25 m, receiver interval 12.5 m, traces 192, minimum offset 12.5 m). The OBS deployment recorded 4C OBS seismic data of a typical 3D seismic survey. Figure 3 shows the survey design and wave propagation. Table 1 shows the acquisition parameters. Downgoing P waves from the sources travel to the seabed and underneath layers. SS, PP, and PS waves were recorded. Typically, P waves do not transform to S waves at the seabed. Therefore, 4C OBS recorded PP and PS waves because the PS waves are much stronger than the SS waves (Zhang et al., 2014b).

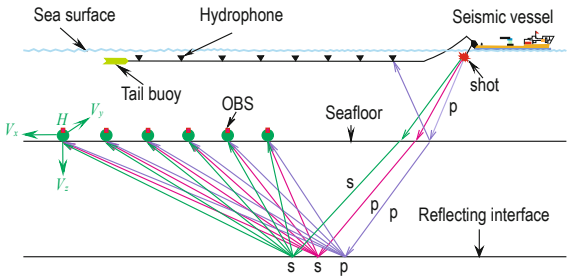

Fig.3 Marine survey and OBS deployment.

Table 1 Acquisition parameters of OBS and 3D streamer survey

Acquisition	Parameters
Shot interval	25 m
OBS interval	400 m–500 m
OBS sample rate	2 ms, 4C
Survey length	18.7 km

Processing procedures

Station repositioning

Owing to the strong water currents, the lack of a navigation system makes it difficult to accurately locate stations. Therefore, relocating stations is mandatory at each step. Relocation computes the X, Y, and Z receiver coordinates from direct arrival picks (Guevara and Stewart, 1998). Direct arrival time picks and shot coordinates are stored in headers with common receiver gathers, and then, they are computed independently for each common receiver gather. The picks are shown in groups of time slices in Figure 4. The time slices of direct arrival waves can be used to estimate the location of OBS (Cantillo et al., 2010). Using all estimated centers, we obtain the final location of OBS statistically.

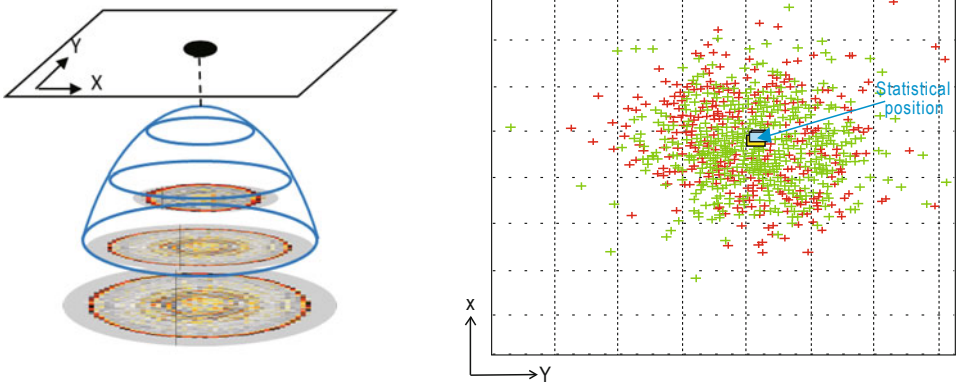

(a) Time slices and estimates of the center (b) Statistical positioning of the center

Fig.4 Schematic diagram of the station relocation.

The positions and shift values of the stations before and after relocation are shown in Figure 5. Maximum shift occurs at station No. 2 and is 160.7 m, whereas the minimum is 11.1 m. The average shift is around 65.1 m. After repositioning, all stations are accurately positioned, which significantly improves the precision of the subsequent reorientation processing.

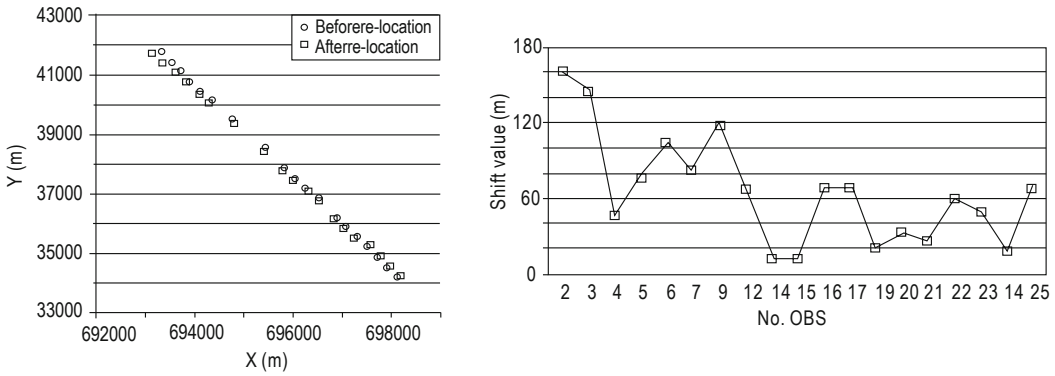

(a) Position of 19 stations before and after relocation (b) Shift for 19 stations

Fig.5 Relocation value for 19 stations.

Reorientation

Relocation ensures that the receivers are correctly positioned (Burch, 2005); moreover, the orientation of the three components needs to be known. The orientation of the stations can be determined by the direct arrival time and QC using the hodogram shown in Figure 6. For residual error values of 90°, the hodogram colors are red, and for residual error values of 0°, the hodogram colors are blue, and the polarization vector points to the receiver. Figure 6a shows the hodogram of station 25 with the sources around it. Prior to reorientation, the polarization direction is random. After reorientation, the polarization points to the source –receiver direction, as shown in Figure 6b; moreover, the 3C data have been rotated from X, Y, and Z to the radial (R), transverse (T), and vertical (V) components. Figure 7 also shows that after reorientation, the major reflection energy from the Y component is transferred to the R and Z components because the energy of P waves is polarized in the propagation plane. The T component is polarized out of the plane, which is characterized by less energy in isotropic media.

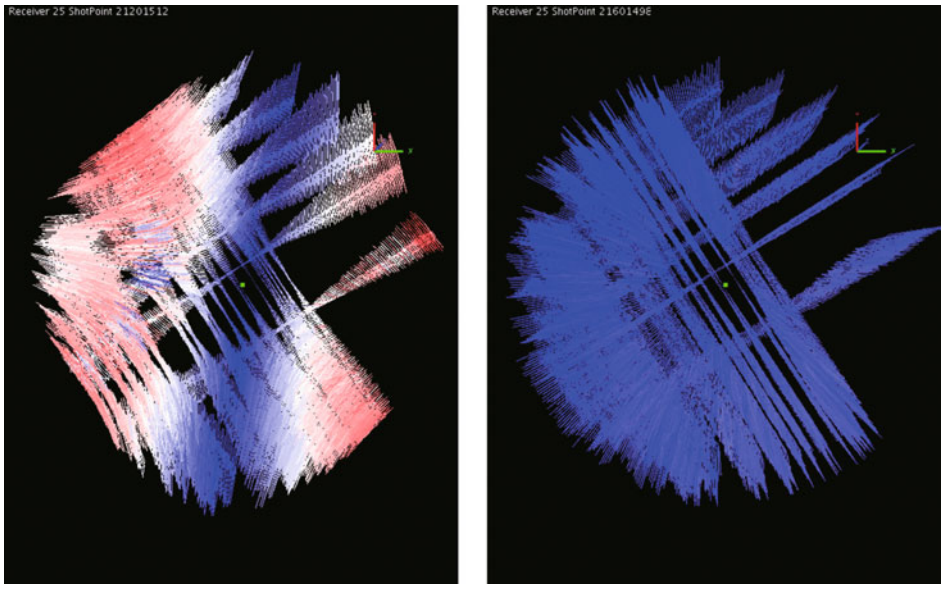

Fig.6 Hodogram before and after reorientation.

The receiver is located at the center and is represented by the green dot. (a) Before reorientation, the hodogram is aligned randomly. (b) After reorientation, the hodogram is aligned in the source–receiver direction. Blue indicates polarization in the source–receiver plane.

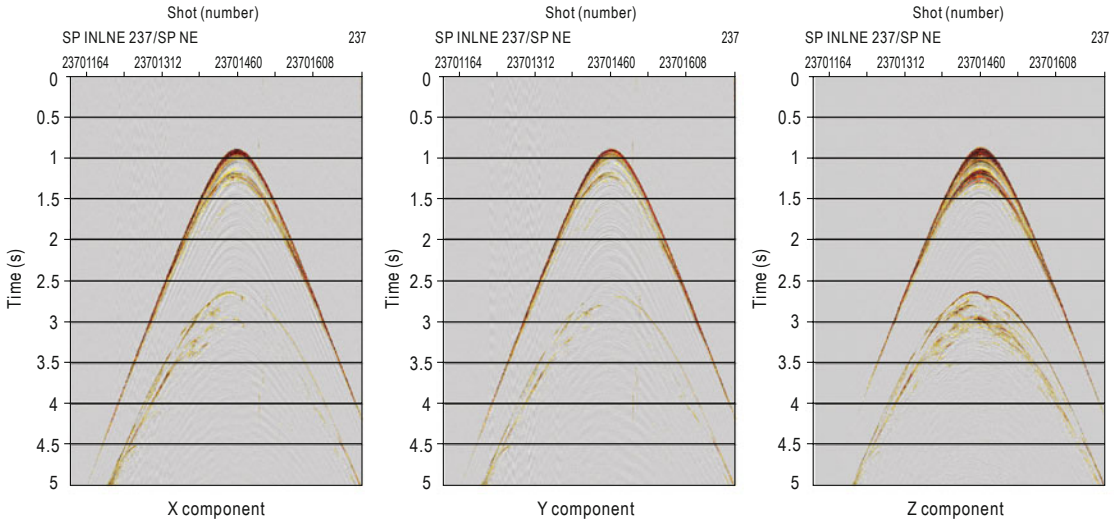

Fig.7 (a) X-, Y-, and Z-component data before reorientation.

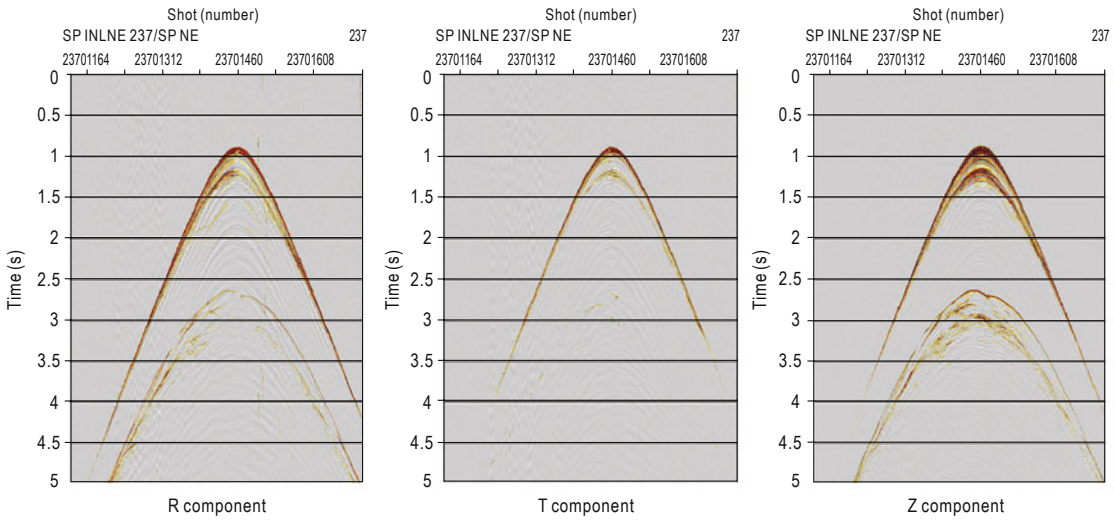

Fig.7 (b) R-, T-, and Z-component data after reorientation.

PZ summation and wavefield separation

After repositioning and reorientation, noise attenuation is applied. Otherwise, noise significantly affects the PZ summation. Once, we obtain clean hydrophone and geophone data, PZ summation is performed to separate the upgoing and downgoing waves, which will be used in imaging. Before summation, geophone data are calibrated using compressional waves to overcome the signal difference from 1) the different recordings for hydrophone and geophone sensors, 2) the coupling difference, and 3) the different sensitivities. After calibrating the geophone data, the separation of upgoing and downgoing waves is achieved by summing and subtracting the calibrated geophone and hydrophone data (Amundsen, 2001; Wang et al., 2010a). During the summation–subtraction procedure, the Z-component dataset is calibrated using the P component. Cross ghosting is a commonly used calibration method (Wang et al., 2010b; Soubaras, 1996). The calibration proceeds by searching for a matching filter between the P and Z components (Hugonnet et al., 2011). Figure 8 shows the PZ-summation results, where Figure 8a shows the P component and Figure 8b shows the calibrated Z component. After summation and subtraction, we obtain upgoing waves (Figure 8b) and downgoing waves (Figure 8d). The upgoing waves contain primary reflections around 1.0–1.4 s. The downgoing waves contain ghost energy in the 2.5–3.2 s range. In the following section, the upgoing wave is used in conventional imaging, and the downgoing wave is used in mirror imaging.

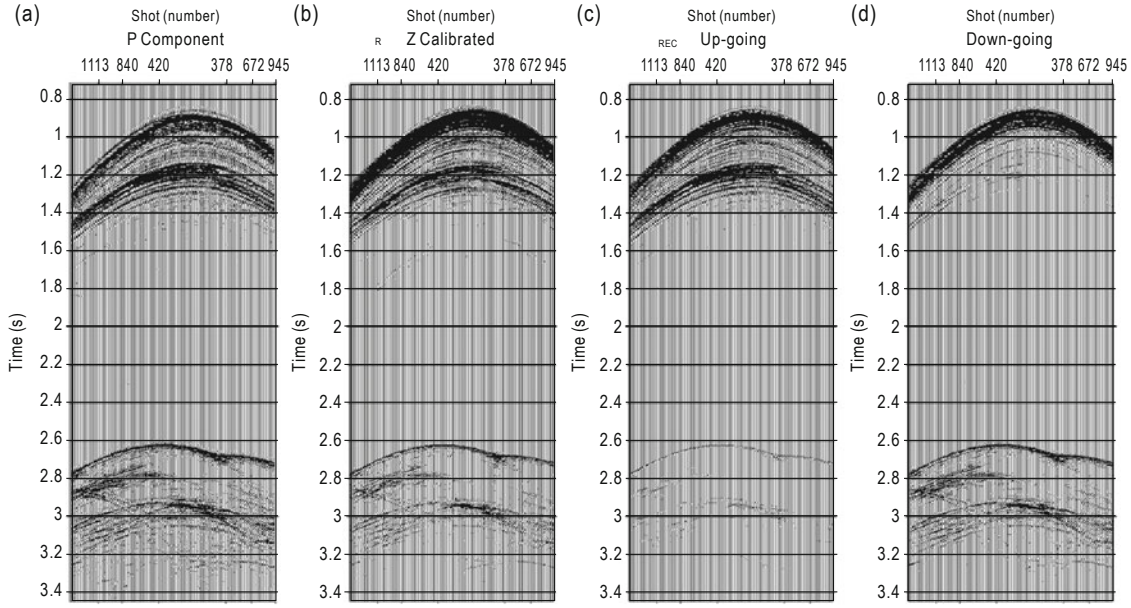

Fig.8 Wavefield separation using PZ summation and subtraction: (a) P component, (b) calibrated Z component, (c) upgoing waves, and (d) downgoing waves.

Mirror Imaging

The acquisition geometry of OBS data is generally characterized by the sparse and localized receiver spread in conjunction with a wide and dense shot grid. As shown in Figure 9a, the sparse spread of the stations provides limited imaging illumination. The situation becomes worse for shallow targets and missing stations. However, with mirror imaging that uses first-order receiver-side sea-surface multiples, both sea floor and shallow structures are much better imaged. Figures 9b and 9c show why mirror imaging offers wider subsurface coverage than conventional migration (Grion et al., 2007).

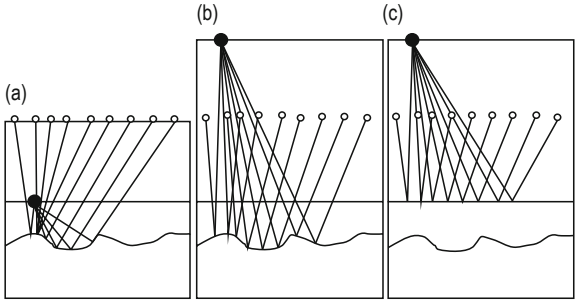

Fig.9 Conventional OBS imaging acquisition and illumination: (a) and (b) mirror OBS location and mirror imaging better illuminates the shallow structures. (c) mirror imaging better illuminates the sea bottom.

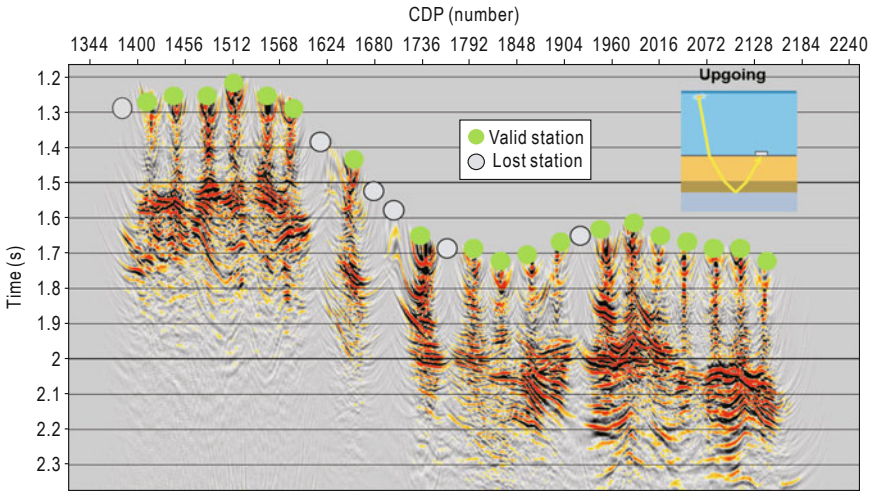

Fig.10 Conventional migration by using upgoing waves from 24 stations. Green dots denote locations of valid stations and black dots denote locations of lost stations. Illumination is limited owing to the sparse separation of stations, especially in the images under the lost stations.

Figure 10 shows conventional imaging of the 19 OBS dataset. Using upgoing waves (primary reflections) can only provide useful information for the deep parts. It is difficult to obtain clear structures for the shallow parts and sea floor owing to the lack of illumination coverage. On the other hand, mirror imaging of the same data, as shown in Figure 11, significantly improves the results for shallow and sea floor structures. In the study area, the gas hydrates are located 500 m beneath the sea floor, as shown in Figure 11. Therefore, mirror migration is critical role in producing images for BSR detection because of the wider illumination angles than conventional migration.

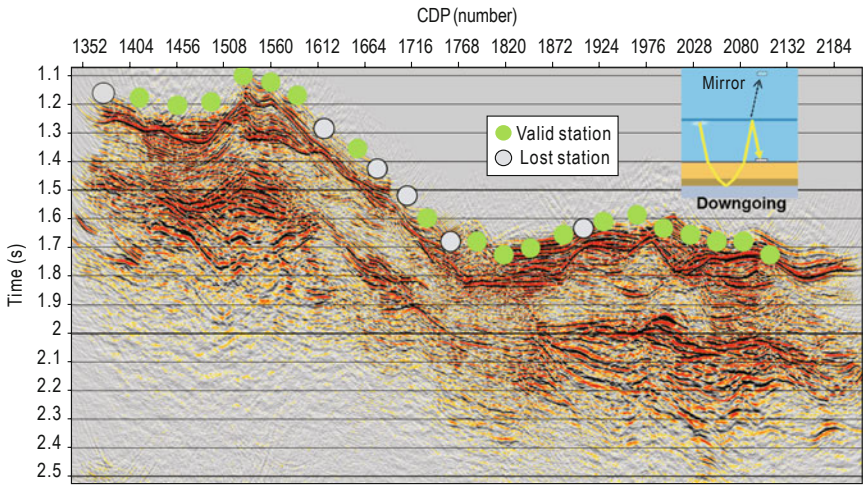

Fig.11 Mirror migration by using downgoing waves from 24 stations. Green dots denote locations of valid stations and black dots denote locations of lost stations. Mirror migration provides a clear image of the sea bottom and shallow section.

Discussion

A problem with OBS is the sparse spatial sampling of the stations (receiver interval 400 m) because of cost. The gathers and conventional imaging are of very poor quality owing to the narrow illumination, and the velocity analysis is challenging because of low and irregular folds. However, we developed a new method for analyzing velocity based on mirror imaging by taking advantage of the better illumination of the receiver ghost from each station. Even at the lost stations, mirror imaging also obtains consistent results in which the energy comes from the nearer stations.

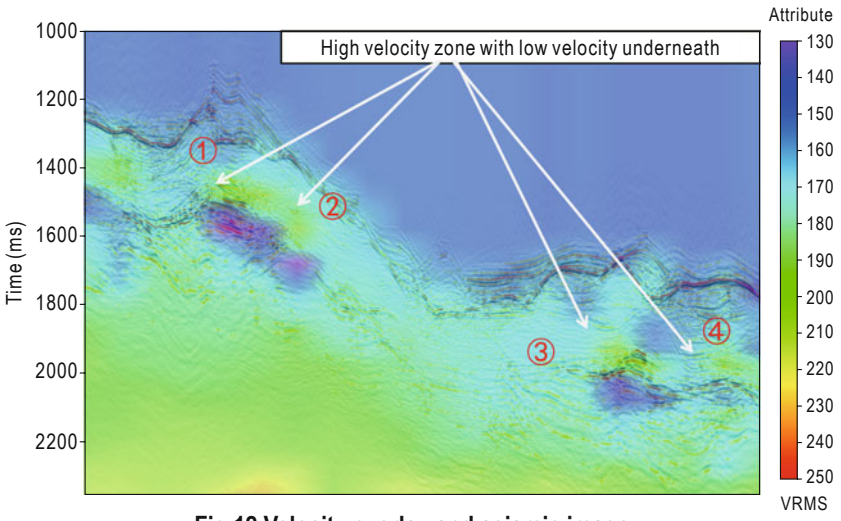

Fig.12 Velocity overlay and seismic image.

Using mirror-imaging stacking, we conduct percent velocity scanning to obtain the RMS velocity that is close to water velocity because of the large water column. From the RMS velocity, we derive the interval velocity by the Dix formula. Figures 12 and 13 show the interval velocity over the seismic image. Four obvious high-velocity zones (green) with low-velocity zones underneath (dark blue zones) successfully match the strong reflection, which is known as BSR. It mimics the seafloor with reversed polarity, and is associated with the base of the gas hydrate stability field (Hyndman and Davis, 1992; Kvenvolden, 1993). Gas trapped underneath the gas hydrate-bearing zone is assumed to cause such strong impedance contrast. The contrast between the upper high-velocity gas hydrate zone and the low-velocity trapped gas zone below assist us in distinguishing the gas hydrate.

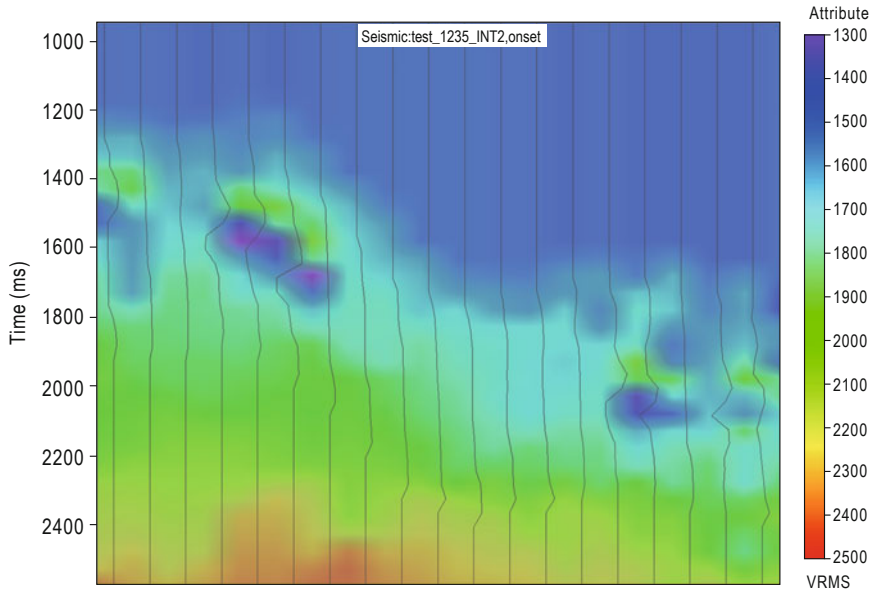

Fig.13 Velocity overlay with station locations in Black Lines.

Conclusions

We processed OBS data to detect BSR and gas hydrates in the northern continental slope of SCS by mirror imaging and other associated technologies. We have shown that OBS data can be used to detect gas hydrates using BSR imaging and velocity modeling. In this case, the OBS data contain high S/N and high-resolution reflections. However, owing to the sparse distribution of the stations, it is difficult to obtain continuous images with conventional methods. Compared with conventional imaging, mirror imaging produces better images of the shallow parts and velocity structures. Station relocation, reorientation, and PZ summation ensure the quality of the migration results. Mirror migration of the downgoing ghost reflections produces better images than conventional migration using upgoing primary reflections. From the imaging results and velocity field, we have successfully identified the BSR. We demonstrated that the OBS technology is an effective solution for BSR characterization in deep waters, and OBS data acquisition can be used to detect gas hydrates, at least in this area.

Acknowledgements

We thank CGG Technology Services (Beijing) Ltd. for data processing. The authors also express their sincere thanks to the Liu Xue-Wei and Song Haibing Professors, and Su Ke-Hua Doctor, whose critical and constructive comments and suggestions greatly improved the final paper.

References

Amundsen, L., 2001, Elimination of free-surface related

multiples without need of a source wavelet: Geophysics, **66**(1), 327−341.

Burch, D. N., Calvert, A. S., and Novak, J. M., 2005, Vector fidelity of land multicomponent measurements in the context of the earth-sensor system: misconceptions and implications: 75th Annual International Meeting, SEG, Expanded Abstracts, 904−907.

Cantillo, J., Boelle, J. L., Lafram, A., and Lecerf, D., 2010, Ocean-bottom nodes (OBN) repeatability and 4D: 80th Annual International Meeting, SEG Expanded Abstracts, 61−65.

Gong, Y. H., Wu, S. G., Zhang, G. X., Wang, H. B., Liang, J. Q., Guo, Y. Q., and Sha, Z. B., 2008, Relation between gas hydrate and geologic structures in dongsha islands area of south china sea: Marina Geology & Quaternary Geology (in Chinese), **28**(1), 99−104.

Grion, S., Exley, R., Manin, M., Miao, X. G., Pica, A., Wang, Y., Granger, P. Y., and Ronen, S., 2007, Mirror imaging of OBS data: First Break, **25**(11), 37−42.

Guevara, S. E., and Stewart, R. R., 1998, Multicomponent seismic polarization analysis: CREWES Research Report, 10.

Hugonnet, P., Boelle, J. L., Herrmann, P., Prat, F., and Lafram, A., 2011, PZ summation of 3D WAZ OBS receiver gathers: 73nd EAGE meeting, Expanded Abstract, 30.

Hyndman, R. D., and Davies, E. E., 1992, A Mechanism for the Formation of Methane Hydrate and seafloor bottom simulating reflectors by vertical fluid expulsion: Journal of Geophysical Research, **97**(B5), 7025−7041.

Kvenvolden, K. A., 1993, Gas hydrates-geological perspective and global change: Reviews of Geophysics, **31**(2), 173−187.

Li, L., Lei, X. H., Zhang, X., and Sha Z. B., 2013, Gas hydrate and associated free gas in the Dongsha Area of northern South China Sea: Marine and Petroleum Geology, **39**(1), 92−101.

Pang, X., Chen, C. M., Peng, D. J., Zhou, D., Shao, L., 2009, Basic Geology of Baiyun deep water area in the North part of Nanhai: China Petroleum Geology Society, 2009, **20**(4), 215−222.

Riedel, M., Spence, D., Chapman, N. R., and Hyndman, R. D., 2001, Deep-sea gas hydrates on the northern cascadia margin: The leading edge, 87−92.

Shi, X. F., and Yan, Q. S., 2011, Geochemistry of Cenozoic magmatism in the South China Sea and its tectonic implications: Marine Geology and Quaternary Geology, **31**, 59−72.

Soubaras, R., 1996, Ocean-bottom hydrophone and geophone processing: Proceedings of the Society of Exploration Geophysicists, 24−27.

Wang, Y., Bale, R., and Grion, S., 2010a, A new approach to remove the water column effect from 4D ocean bottom data: 80th SEG Annual Meeting, 4205−4209.

Wang, Y., Grion, S., and Bale, R., 2010b, Up-down deconvolution in the presence of subsurface structure, 72nd EAGE meeting, Expanded Abstract, D001.

Yi, H., Zhong, G. J., and MA, J. F., 2007, Fructure characteristics and basin evlution of the Taixinan basin in genozoic: Petroleum Geology & Experiment (in Chinese), **29**(6), 560−564.

Zhang, G. X., Liang, J. Q., LU J. A., Yang, S. X., Zhang, M., Su, X., Xu, H. N., Fu, S. Y., and Kuang, Z. G., 2014a, Characteristics of natural gas hydrate reservoirs on the northeastern slope of the South China Sea: Natural gas industry (in Chinese), **34**(11), 1−10.

Zhang, G. X., Xu, H. N., Liu, X. W., Zhang, M., Wu, Z. L., Liang, J. Q., Wang, H. B., and Sha, Z. B., 2014b, The acoustic velocity characteristics of sediment with gas hydrate revealed by integrated exploration of 3D seismic and OBS data in Shenhu area: Chinese Journal of Geophysics (in Chinese), **57**(4), 1169−1176.

Sha Zhi-Bin graduated from China University of Geosciences (Wuhan) in June 1994. He is a presently a PHD. student in the Department of Marine Geology, Faculty of Resources, China University of Geosciences (Wuhan). His research interests are seismic surveying of gas hydrates. Email: shazb2008@163.com.